Cl-Loss Dynamics of Vinyl Chloride Cations in the B²A″ State: Role of the C²A′ State

Xiangkun Wu,[†,∥] Manman Wu,[†,∥] Xiaofeng Tang,[†] Xiaoguo Zhou,*,[†,‡] Shilin Liu,[†,‡] Fuyi Liu,[§] and Liusi Sheng[§]

[†]Hefei National Laboratory for Physical Sciences at the Microscale and Department of Chemical Physics and [‡]Synergetic Innovation Center of Quantum Information & Quantum Physics, University of Science and Technology of China, Hefei, Anhui 230026, China

[§]National Synchrotron Radiation Laboratory, University of Science and Technology of China, Hefei, Anhui 230029, China

Ⓢ *Supporting Information*

ABSTRACT: The dissociative photoionization of vinyl chloride (C_2H_3Cl) in the 11.0−14.2 eV photon energy range was investigated using threshold photoelectron photoion coincidence (TPEPICO) velocity map imaging. Three electronic states, namely, A^2A', B^2A'', and C^2A', of the $C_2H_3Cl^+$ cation were prepared, and their dissociation dynamics were investigated. A unique fragment ion, $C_2H_3^+$, was observed within the excitation energy range. TPEPICO three-dimensional time-sliced velocity map images of $C_2H_3^+$ provided the kinetic energy release distributions (KERD) and anisotropy parameters in dissociation of internal-energy-selected $C_2H_3Cl^+$ cations. At 13.14 eV, the total KERD showed a bimodal distribution consisting of Boltzmann- and Gaussian-type components, indicating a competition between statistical and non-statistical dissociation mechanisms. An additional Gaussian-type component was found in the KERD at 13.65 eV, a center of which was located at a lower kinetic energy. The overall dissociative photoionization mechanisms of $C_2H_3Cl^+$ in the B^2A'' and C^2A' states are proposed based on time-dependent density functional theory calculations of the Cl-loss potential energy curves. Our results highlight the inconsistency of previous conclusions on the dissociation mechanism of $C_2H_3Cl^+$.
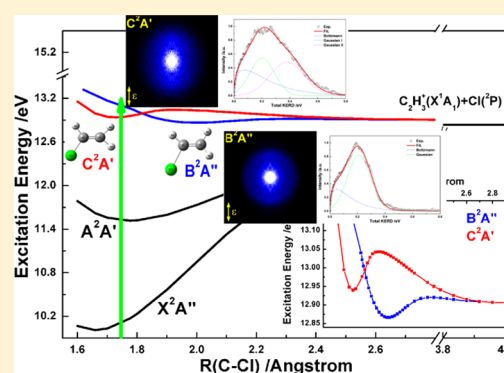
1. INTRODUCTION

Vinyl chloride (C_2H_3Cl) is an important intermediate reagent in the chemical industry, and its reactions have been extensively studied. The neutral C_2H_3Cl molecule in the ground electronic state has a planar structure with C_s symmetry. Removing an electron from its outer orbitals, such as the $3a''$, $13a'$, $2a''$, and $12a'$ orbitals, produces a $C_2H_3Cl^+$ cation in one of several possible electronic states, including X^2A'', A^2A', B^2A'', and C^2A'. The spectroscopy of $C_2H_3Cl^+$ cation has been extensively investigated.[1−10] In photoelectron spectroscopy (PES)[7,8] and threshold photoelectron spectroscopy (TPES),[9] a series of vibrational bands were observed for the X^2A'' and A^2A' states, while the B^2A'' and C^2A' bands were structureless and severely overlapped. The adiabatic ionization energy of C_2H_3Cl was determined to be 10.0062 ± 0.0003 eV using high-resolution zero-kinetic-energy (ZEKE) PES.[10] The ionization energy of the A^2A' and B^2A'' states was measured using mass-analyzed threshold ionization (MATI)[11] and MATI photodissociation yield (PDY) spectroscopy.[12] In the MATI-PDY spectrum, several vibrational peaks were observed in the lower-energy region of the B^2A'' state, implying that the ionic state has a shallow potential well.[12]

The photodissociation dynamics of $C_2H_3Cl^+$ cation has not been investigated as intensively as its spectroscopic properties. The ground-state $C_2H_3Cl^+$ cation is stable, and its A^2A' state
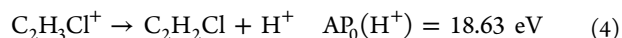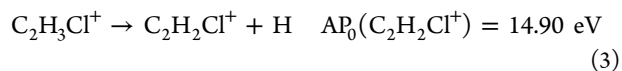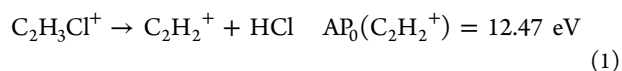
has a long lifetime (tens of microseconds or longer).[13] Concerning its thermochemistry, five dominant dissociation pathways (1−5) exist for $C_2H_3Cl^+$ in its excited electronic states. When synchrotron radiation was used as a photoionization light source, rough appearance energy (AP_0) values of 12.47, 12.54, 14.90, 18.63, and 19.30 eV were obtained for $C_2H_2^+$,[14] $C_2H_3^+$, $C_2H_2Cl^+$, H^+, and Cl^+,[17] respectively, from photoionization efficiency curves.[14−17] $C_2H_3^+$, $C_2H_2^+$, and very few $C_2H_2Cl^+$ fragment ions were observed by Shuman et al. at excitation energies below 13.5 eV using threshold photoelectron photoion coincidence (TPEPICO).[18] The adiabatic dissociation limit for $C_2H_3Cl^+ \rightarrow C_2H_3^+(X^1A') + Cl(^2P)$ was accurately determined to be 12.530 ± 0.010 eV.[18] Kim and co-workers prepared $C_2H_3Cl^+$ in the X^2A'' and A^2A' states by charge exchange, electron impact ionization, and MATI, and then observed the dissociation pathways under UV photoexcitation (461−403 nm) using mass-analyzed ion kinetic energy spectrometry (MIKES)[19] and MATI-PDY spectroscopy.[12] Analysis of the time-of-flight (TOF) profile of the $C_2H_3^+$ fragment led to two suggested dissociation mechanisms for $C_2H_3Cl^+$ in the B^2A'' state: internal conversion to X^2A'' state,

followed by a statistical dissociation, and curve-crossing to a repulsive state followed by direct dissociation.

$$C_2H_3Cl^+ \rightarrow C_2H_2^+ + HCl \quad AP_0(C_2H_2^+) = 12.47 \text{ eV} \tag{1}$$

$$C_2H_3Cl^+ \rightarrow C_2H_3^+ + Cl \quad AP_0(C_2H_3^+) = 12.53 \text{ eV} \tag{2}$$

$$C_2H_3Cl^+ \rightarrow C_2H_2Cl^+ + H \quad AP_0(C_2H_2Cl^+) = 14.90 \text{ eV} \tag{3}$$

$$C_2H_3Cl^+ \rightarrow C_2H_2Cl + H^+ \quad AP_0(H^+) = 18.63 \text{ eV} \tag{4}$$

$$C_2H_3Cl^+ \rightarrow C_2H_3 + Cl^+ \quad AP_0(Cl^+) = 19.30 \text{ eV} \tag{5}$$

A few theoretical calculations have been performed to investigate the dissociation dynamics of $C_2H_3Cl^+$. Potential energy curves of the low-lying electronic states of $C_2H_3Cl^+$ in planar C_s symmetry were calculated using a complete active space self-consistent field (CASSCF) and multiconfiguration second-order perturbation theory (CASPT2).[20] The X^2A'', A^2A', and B^2A'' states were bound, while the C^2A' ionic state was reported to be repulsive. A curve-crossing between the B^2A'' and C^2A' states was suggested to cause dissociation of $C_2H_3Cl^+(B^2A'')$ cation by Lee and Kim.[12] However, crossing of the potential energy surfaces in C_s symmetry may lead to a symmetry-allowed conical intersection in C_1 symmetry. Yamaguchi applied the CASSCF multireference configuration interaction (MRCI) method to recalculate the potential energy curves of $C_2H_3Cl^+$ in different ionic states.[21] The avoided crossing caused the potential energy curve of B^2A'' state to show a small barrier at $R(C-Cl) = 2.4-2.5$ Å along the $C_2H_3^+(X^1A_1) + Cl(^2P)$ dissociation channel. The barrier height was only 1400 cm^{-1} at the MRCISD+Q level of theory, above which a Cl atom was ejected out of the vinyl plane.[21] The conical intersection between the B^2A'' and C^2A' states had a higher energy than the barrier of B^2A'', and thus dissociation of B^2A'' tends to proceed adiabatically. Both potential energy curves are plotted in the Supporting Information (Figure S1) and were obtained by reading the points of an enlarged copy of the published figures. Obviously, the conclusions of both previous calculations on the dissociation mechanism of B^2A'' are different.

Although some experimental and theoretical investigations have been performed to describe the dissociation of $C_2H_3Cl^+$, uncertainties remain. Especially, the C^2A' state probably plays a significant role in dissociation of the nearby B^2A'' state. However, its dissociation has not been investigated in an experiment until now. As an upgraded experimental technique, TPEPICO velocity map imaging is a very powerful technique for investigating the dissociation dynamics of internal-energy-selected ions.[22−26] A lot of new dissociation information on molecular ions has been successfully obtained,[27−33] for example, dark state, vibrational dependence, mass effect, and so on.

In this work, the dissociation of internal-energy-selected $C_2H_3Cl^+$ is investigated using TPEPICO velocity map imaging in the excitation energy range of 11.0−14.2 eV, where the A^2A', B^2A'', and C^2A' ionic states are involved. Kinetic energy release distributions and anisotropy parameters of $C_2H_3^+$ fragment ion are directly obtained from TPEPICO images at the different electronic excited states of $C_2H_3Cl^+$. Special attention is paid to the branching ratio of the statistical and non-statistical dissociation pathways. A new theoretical calculation based on

time-dependent density functional theory (TDDFT) is performed, and the shallow wells are located on the potential energy surfaces of B^2A'' and C^2A' excited states in the Franck−Condon region. Thus, the C^2A' excited state is suggested to be bound rather than repulsive. On the basis of theoretical and experimental conclusions, the C−Cl bond rupture mechanisms of $C_2H_3Cl^+$ cation in B^2A'' and C^2A' excited states are proposed.

2. EXPERIMENTAL AND COMPUTATION

The present experiments were performed on the U14-A undulator beamline of the National Synchrotron Radiation Laboratory located at Hefei, China. The detailed configurations of the beamline and TPEPICO velocity imaging spectrometer have been reported previously,[22] and so only a brief description is presented here. Synchrotron radiation from the 800 MeV electron storage ring was dispersed with a 6 m vacuum ultraviolet (VUV) monochromator, where grating having 370 grooves·mm^{-1} was used to cover the photon energy range of 7.5−22.5 eV. A gas filter filled with a noble gas was used to absorb the higher-order harmonic radiation of beamline. In the present experiment, the energy-resolving power of the monochromator was ∼2000 of $E/\Delta E$. The absolute energy of VUV photons was carefully calibrated in TPES experiments using the well-known ionization energies of noble gases like argon and neon, and a silicon photodiode (International Radiation Detectors Inc., SXUV-100) was used to record photon flux.
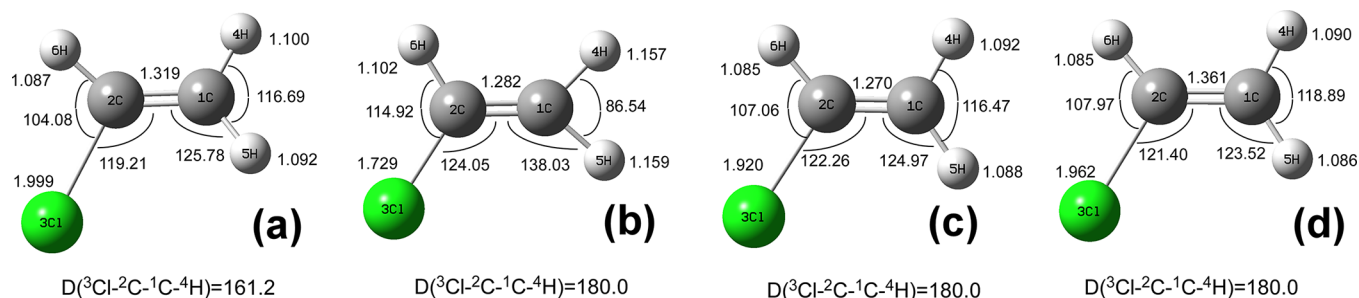
A commercial C_2H_3Cl/Ne gas mixture with a volume ratio of 20% (stagnation pressure of 1.2 atm) was used as the sample. It was injected into a source chamber through a 30 μm diameter nozzle to generate a continuous supersonic molecular beam. After it was skimmed by a 0.5 mm diameter skimmer, the molecular beam was intersected with synchrotron light at 10 cm downstream from the nozzle in the photoionization chamber. The source and photoionization chambers were pumped, respectively, by 1800 and 1600 L·s^{-1} turbo-molecular pumps. The typical background pressure in the photoionization chamber was ∼1 × 10^{-4} Pa with the molecular beam on.

In the present TPEPICO spectrometer, double velocity map imaging[22] was applied to collect and detect threshold electrons and cations simultaneously. Photoelectrons and photoions were separated by a direct current extraction field (∼14 V·cm^{-1}), and each of their velocity images was projected in opposite directions. A decelerated electric field was utilized to magnify and map the velocity image of electrons. Moreover, a mask with a 1 mm diameter aperture was located just in front of the electron detector, and electrons passing through the aperture were identified as the threshold photoelectrons. Although the contamination of hot electrons (with a certain kinetic energy) was efficiently suppressed by the magnification of the velocity map image, the hot electrons with the initial velocity along the TOF direction could still inevitably pass through the hole and be falsely collected as the threshold electrons. Thus, an additional method similar to the previously reported subtraction[34] was necessary to further reduce the false coincidence. Unlike the detection of electrons, velocity map images of photoions were directly projected on two 40 mm diameter multichannel plates backed by a phosphor screen (Burle Industries, P20). A thermoelectric cooling charge-coupled device camera (Andor, DU934N−BV) was used to record the image on the screen. In the present coincident experiment, a pulsed high voltage (DEI, PVM-4210) was applied at the

Table 1. Optimized Geometries, Vertical (T_v) and Adiabatic (T_0) Ionization Energies of $C_2H_3Cl^+$ Cation in X^2A'', A^2A', B^2A'', and C^2A' States, and the Geometry Parameters of Neutral C_2H_3Cl Molecule in Ground State (X^1A')

state	R(C–C), Å	R(C–Cl), Å	A(^{1}C–^{2}C–^{6}H)[a]	T_v, eV[b]		T_0, eV[b]	
				cal	exp	cal	exp
$X^2A''(C_s)$	1.395	1.659	122.54	10.10	10.005[d]	9.81	10.0062[e]
	1.405[c]	1.657[c]	122.5[c]	9.631[c]			
	1.392[e]	1.657[e]	122.4[e]				
	1.391[f]	1.640[f]	122.6[f]				
$A^2A'(C_s)$	1.326	1.775	128.41	11.75	11.664[d]	11.74	11.6667[e]
	1.327[f]	1.752[f]	131.2[f]	11.141[c]			
$B^2A''(C_1)$	1.319	1.999	135.74	13.07	13.13[d]	12.84	12.7518[e]
	1.368[c]	1.964[V]	131.6[c]	12.596[c]			
	1.316[e]	1.991[e]	135.6[e]				
	1.354[f]	1.937[f]	131.4[f]				
$C^2A'(C_s)$	1.282	1.729	121.03	13.57	13.56[d]	13.17	
				13.422[c]			
$X^1A'(C_s)$	1.324	1.752	124.40				
	1.332[g]	1.726[g]	123.8[g]				

[a]C=C−H bond angle (degrees) in vinyl cation moiety. [b]Ionization energies were calculated with the optimized geometry of ground neutral molecule. [c]SA-CASSCF optimized geometries and MRCISD energies from ref 21. [d]From He(I) photoelectron spectra of ref 9. [e]From MATI-PFY spectra of ref 12. [f]CASPT2 geometries from ref 20. [g]Experimental data from ref 42.

D(^{3}Cl-^{2}C-^{1}C-^{4}H)=161.2   D(^{3}Cl-^{2}C-^{1}C-^{4}H)=180.0   D(^{3}Cl-^{2}C-^{1}C-^{4}H)=180.0   D(^{3}Cl-^{2}C-^{1}C-^{4}H)=180.0

Figure 1. Optimized geometries of the B^2A'' (a) and C^2A' (b) states, and the conical intersection (c) between B^2A'' and C^2A' states at TD-DFT B3LYP/6-311+G(d,p) level. The optimized planar structure of B^2A'' state (d).

microchannel plates of the ion detector as a mass gate (∼40 ns) to detect a time-sliced velocity map image of the coincident ions.

All theoretical calculations were performed with Gaussian 09W program package (D.01 version 9.5).[35] Geometries of neutral C_2H_3Cl and its ground-state cation were optimized with density functional theory (DFT) at the B3LYP/6-311+G(d,p) level of theory. The optimized geometries of electronic excited states of $C_2H_3Cl^+$ were calculated using TDDFT with a 6-311+G(d,p) basis set. A partial optimization method was applied to obtain the Cl-loss potential energy curves of the electronic states, in which the lowest eight electronic states (five of A′ and three of A″ states in C_s symmetry) were involved. At every given C−Cl distance, the other geometry parameters were reoptimized. The electronic configuration of the ionic state was carefully checked to confirm symmetries in the open-shell excited species. Using the DFT-optimized geometries, the vertical and adiabatic ionization energies of the ionic states were calculated at the EOM-CCSD/cc-PVTZ level.[36−39]

3. RESULTS AND DISCUSSION

3.1. Optimized Geometries of $C_2H_3Cl^+$ in Low-Lying Electronic States.
Table 1 summarizes the optimized geometries and vertical and adiabatic ionization energies of $C_2H_3Cl^+$ in its X^2A'', A^2A', B^2A'', and C^2A' states. The results for the X^2A'' and A^2A' states are consistent with previous

calculations and experimental data. However, in the present calculation, the optimized structure of the B^2A'' state is nonplanar, while those of the X^2A'', A^2A', and C^2A' states are planar. Figure 1a,b shows the optimized geometries of B^2A'' and C^2A' states, where the dihedral angle D(^{3}Cl−^{2}C−^{1}C−^{4}H) is 161.2° for B^2A'' and 180° for C^2A'. The C−Cl bond length is elongated to 2.00 Å, and the bond angle θ(^{1}C−^{2}C−^{6}H) is increased to 135.74° after photoionization to the B^2A'' state, while the other parameters are close to those in neutral C_2H_3Cl. Thus, the potential well of the twisted B^2A'' state is far from the Franck−Condon region. In addition, a planar structure of B^2A'' was also optimized with a restriction of C_s symmetry, and it is exhibited in Figure 1d. The geometry looks very similar to the previous MRCI structure shown in Table 1, implying that the present calculation is accurate enough to predict molecular ion structures. The C^2A' state has a similar planar geometry to that of the ground state of neutral C_2H_3Cl, except for the short C−C bond length. Thus, the original band of C^2A' state in TPES is expected to show a relatively high intensity when direct photoionization occurs.

It is worth noting that a planar optimized geometry was incorrectly assigned as B^2A'' in Yamaguchi's calculation,[21] where the C−C bond length (1.368 Å) was much larger than the present result (1.319 Å). A similar planar geometry was obtained for the B^2A'' state in Chang et al.'s CASPT2 calculations with restriction of C_s symmetry.[20] This incorrect
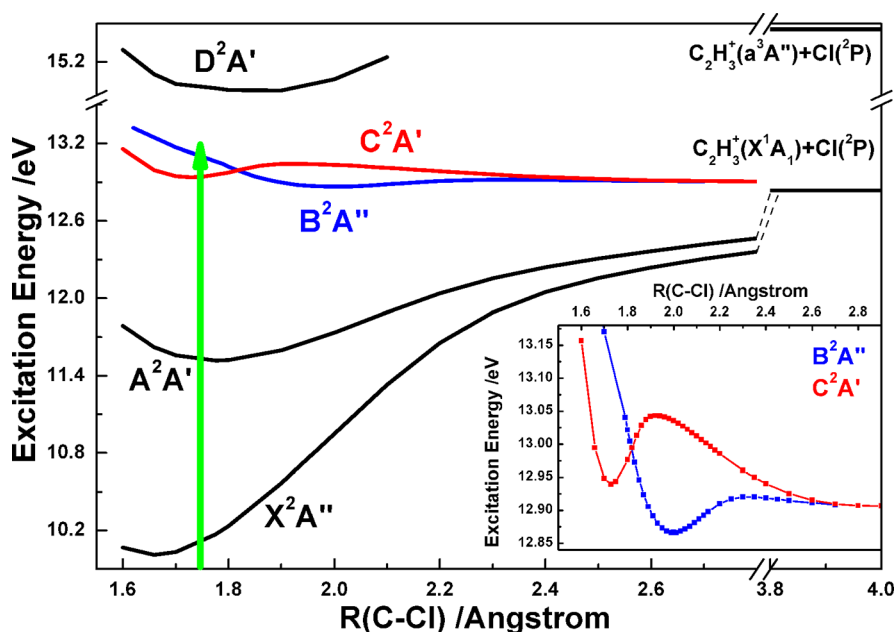
Figure 2. Cl-Loss adiabatic potential energy curves of low-lying electronic states of $C_2H_3Cl^+$ at TD-B3LYP/6-311+G(d,p) level, where the green arrow shows the Franck−Condon ionization region from the neutral molecule.

assignment led to an incorrect estimate of the adiabatic excitation energy of B^2A'' by Yamaguchi. As shown in Table 1, the present EOM-CCSD ionization energies based on the TDDFT optimized structure agree very well with the experimental values and are closer to the available experimental data than the previous MRCI calculations,[20,21] implying that the present calculation method is reliable. A probable potential reason for the failure of the previous MRCI computations is that there was insufficient active space for electronic configurations. To further confirm the twisted geometry of B^2A'' state, we performed a frequency calculation for the planar B^2A'' state suggested by Yamaguchi, and an imaginary frequency relating to a twist vibrational mode along C−C bond was found.

3.2. Cl-Loss Potential Energy Curves of $C_2H_3Cl^+$ in Low-Lying Electronic States. As mentioned above, the previous theoretical calculations did not provide a consistent description of the role of the C^2A' state in the dissociation of the B^2A'' state.[20,21] Under planar symmetry, the curve-crossing between the B^2A'' and C^2A' states led to dissociation of the bound B^2A'' state.[20] When taking a variation of the planar geometry in dissociation, the potential energy curve of the B^2A'' state adiabatically correlated to the $C_2H_3^+(X^1A_1)$ + $Cl(^2P)$ dissociation limit with a small barrier according to the interaction of the C^2A' state.[21] However, the potential energy curves of the B^2A'' and C^2A' states in the Franck−Condon region were not calculated in either previous computation. A recent calculation of the potential energy curves of $C_2H_3F^+$ showed that there are very complicated conical intersections between its B^2A'' and C^2A' ionic states.[40,41] Therefore, similar interactions are believed to exist among the electronic states of $C_2H_3Cl^+$ cation as well in the Franck−Condon region.

Although the TDDFT method is based on a single reference configuration, the potential energy curves of electronic excited states can be clearly described for $C_2H_3F^+$.[40,41] Thus, we expected to obtain an analogous mechanism by applying TDDFT to $C_2H_3Cl^+$. Figure 2 shows the calculated adiabatic potential energy curves of low-lying electronic states along the

C−Cl distance. The calculated curves in Figure 2 are vertically offset by 0.2 eV to match the experimental excitation energies. The offset was estimated from the difference of adiabatic excitation energy between the calculated and experimental values.

Both the X^2A'' and A^2A' states are bound and adiabatically correlate with the $C_2H_3^+(X^1A_1)$ + $Cl(^2P)$ channel. These conclusions are consistent with the MRCI calculation.[20,21] The optimized C−Cl bond length of the twisted B^2A'' state is 2.00 Å, and thus its potential well is far from the Franck−Condon region. Along the distance between C and Cl atoms, a very small barrier exists at 2.35 Å with a height of ∼0.06 eV, and the adiabatic products are $C_2H_3^+(X^1A_1)$ and $Cl(^2P)$ as well. The C^2A' state also adiabatically correlates with the $C_2H_3^+(X^1A_1)$ + $Cl(^2P)$ production via a barrier of 0.10 eV height at R(C−Cl) = 1.92 Å. As indicated in the potential energy curves, a conical intersection exists between the B^2A'' and C^2A' states. By loosely scanning the potential energy surface, the conical intersection is roughly located and shown in Figure 1c. The C−Cl bond length is slightly reduced from that of B^2A'' to 1.92 Å at the conical intersection, which is far from the Franck−Condon region. The energy of the conical intersection is only 0.13 eV above the minimum of B^2A'' state at EOM-CCSD/cc-PVTZ level.

As indicated by the vertical excitation energies in Table 1, the C^2A' state is only 0.5 eV higher than B^2A'', and consequently the corresponding bands in TPES naturally overlap, in agreement with the experimental spectra. More importantly, a very shallow well with a height of 0.06 eV was present on the Cl-loss potential energy curve of the B^2A'' state, which is much lower than the previous MRCISD value (1400 cm^{-1}, 0.17 eV). In the MATI-PDY spectrum,[12] only a few vibrational bands were observed just above the band origin of B^2A'', and the vibrational bands with an energy of 598 cm^{-1} (0.07 eV) beyond the band origin were apparently broadened by dissociation. These experimental phenomena are consistent with our calculations, implying that the present calculations are capable
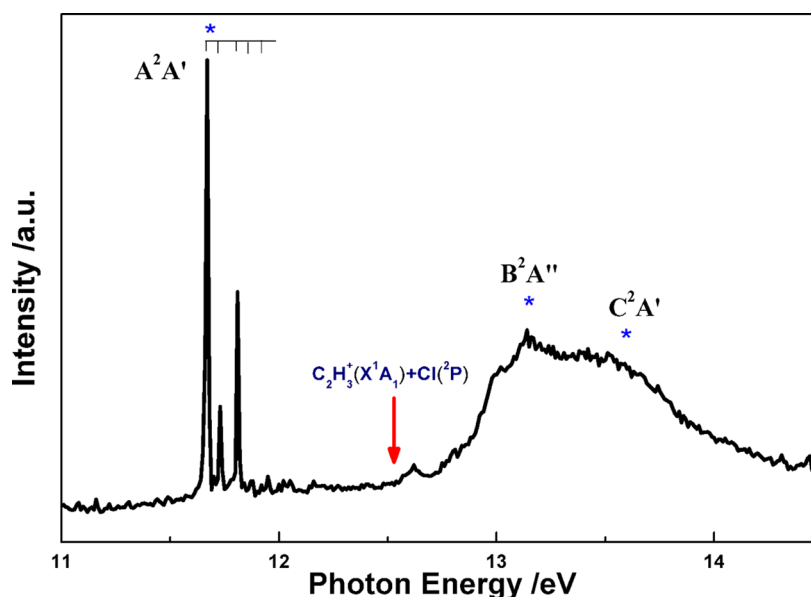
Figure 3. Threshold photoelectron spectrum of C_2H_3Cl in the photon energy range of 11.0−14.5 eV, where the red arrow shows the dissociation limit of $C_2H_3^+(X^1A_1)$ + $Cl(^2P)$. Three asterisks correspond to ionization energies of 11.67, 13.14, and 13.65 eV, where the TPEPICO velocity map images of $C_2H_3^+$ fragments are recorded.

of accurately predicting the characteristics of potential energy curves.

We emphasize that the Cl-loss potential energy curves of B^2A'' and C^2A' states in the previous computations[20,21] are calculated from 2.0 Å of the C−Cl bond length onward, and are thus far from the Franck−Condon region (seen in Figure S1 and S2 of the Supporting Information). The omission of the potential well of the planar C^2A' state led Chang et al. to conclude incorrectly that the C^2A' state was repulsive.[20] Thus, we recalculated the Cl-loss potential energy curves of B^2A'' and C^2A' states with planar symmetry and present the results in Figure S2 of the Supporting Information to facilitate comparison with the previous calculations. In summary, the B^2A'' state is bound in the planar C_s symmetry as Chang et al. suggested, and adiabatically correlates with the higher dissociation limit of $C_2H_3^+(a^3A'')$ + $Cl(^2P)$.[20]

3.3. Threshold Photoelectron Spectrum of C_2H_3Cl. The 14 V·cm^{-1} extraction electric field used in the experiment meant that the energy resolution of threshold photoelectrons was ∼9 meV (full-width half-maximum in TPES).[22] After subtracting the contamination of hot electrons,[34] the TPES of C_2H_3Cl was measured with an energy step of 10 meV in the excitation energy range of 11.0−14.5 eV and is presented in Figure 3. Three electronic excited states of the $C_2H_3Cl^+$ cation, namely, A^2A', B^2A'', and C^2A', are involved. A series of sharp peaks is observed in the energy range of 11.6−12.1 eV, which are assigned to the vibrational bands of the A^2A' state based on previously reported conclusions.[9,11] The peak with a maximum intensity at 11.670 eV is assigned to the origin band of the A^2A' state. The ν_6 (C−H−H rock), ν_8 (C−Cl stretching), and ν_9 (C−C−Cl bend) vibrational modes are also populated. All the intensities and resonant energies of these vibrational bands are consistent with the previous PES and TPES conclusions,[9] but these spectral data are not listed here, because the A^2A' state is outside the scope of this work.

The dominant dissociation pathway of $C_2H_3Cl^+$ ion at the lower energy is to form the $C_2H_3^+(X^1A_1)$ fragment and a $Cl(^2P)$ atom, and its dissociation limit is 12.530 eV.[18] At the

energy of 12.53 eV in Figure 3, the overlap between the B^2A'' and C^2A' states consists of a structureless and broad peak up to 14.5 eV. As for previously reported spectra,[9] the peak can be divided into two parts, whose centers are located at ∼13.14 and 13.51 eV, respectively. As mentioned above, the original band of the C^2A' state in TPES is expected to have a relatively high intensity under direct photoionization. Thus, the B^2A'' state is the only contributor to the lower-energy component in TPES, and the higher-energy component is composed of the C^2A' state, together with the highly vibrationally excited B^2A'' state. Thus, the B^2A'' state of $C_2H_3Cl^+$ is dominantly produced at 13.14 eV. Additionally, the relative intensities of two components are lower in magnitude than those of previously reported TPES.[9] As the energetic electrons are suppressed efficiently, the relative intensity of the B^2A'' and C^2A' bands presented herein should be more reliable than those in previous TPES.[9] In fact, the counts of threshold photoelectrons in the Franck−Condon gap between the A^2A' and B^2A'' states are much lower than those in the previous TPES.[9]

A few vibrational bands were observed near the band origin of B^2A'' in the MATI-PDY spectrum.[12] However, no vibrational bands are observed in Figure 3, except for a weak peak at 12.62 eV that is attributed to the ionization of residual water. This stark difference is thought to be the different Franck−Condon factors. In the MATI-PDY experiment, $C_2H_3Cl^+$ was excited into the B^2A'' state from the ground ionic state. However, the photoionization in the present experiment occurs by direct excitation from the ground state of the neutral molecule. As listed in Table 1, the optimized geometries of the neutral and ionic ground states are somewhat different, especially the C−C and C−Cl bond lengths. Therefore, different Franck−Condon factors are expected, but these factors are not calculated in the present investigation due to autoionization of the high-Rydberg state. Moreover, the existence of a limited vibrational structure in TPES is more consistent with the nonplanar geometry, where the potential well is much shallower than that in C_s symmetry.
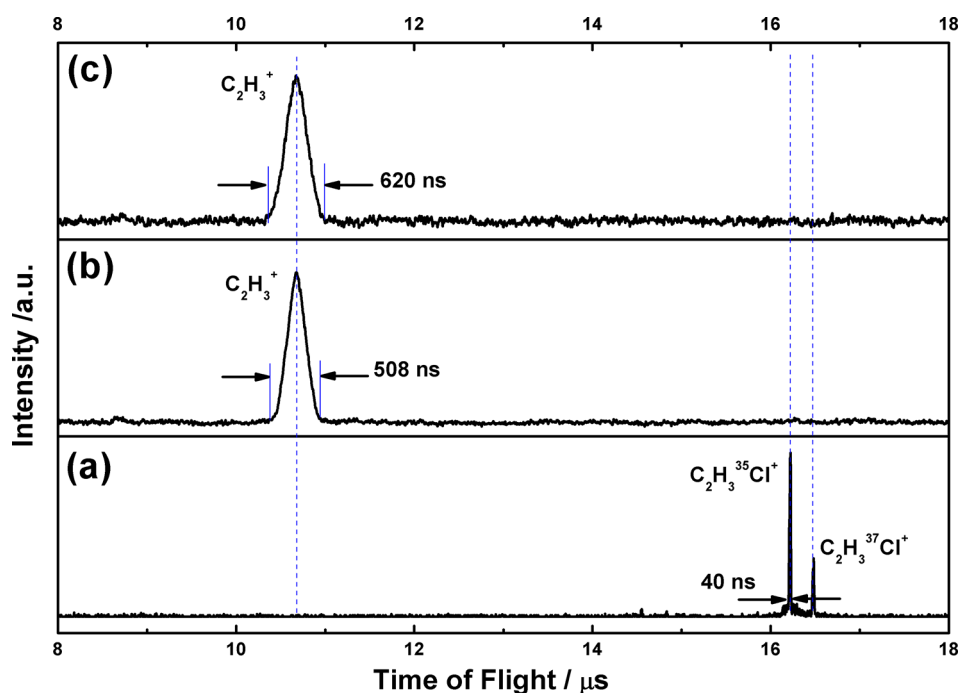
Figure 4. TPEPICO TOF mass spectra of the photoionization of C_2H_3Cl at (a) 11.67, (b) 13.14, and (c) 13.65 eV, where the extraction electric field is 14 V·cm^{-1}.

3.4. TPEPICO Time-of-Flight Mass Spectra.

TPEPICO TOF mass spectra at three typical photon energies of 11.67, 13.14, and 13.65 eV were recorded to detect the fragment ions dissociated from $C_2H_3Cl^+$ at various electronic states. Figure 4 shows mass spectra measured with an extraction electric field of 14 V·cm^{-1}. Since the A^2A' ionic state has a long lifetime,[13] only two parent ions ($C_2H_3{}^{35}Cl^+$, m/z = 62 and $C_2H_3{}^{37}Cl^+$, m/z = 64) are observed at 16.21 and 16.48 μs. The full-width of parent $C_2H_3Cl^+$ cation peaks are 40 ns. Moreover, no dimer or trimer ions were observed near the ionization energy of C_2H_3Cl, although a supersonic expansion was used.

$C_2H_3Cl^+$ in the B^2A'' state is produced at 13.14 eV. As shown in Figure 4b, a unique peak with a center at 10.67 μs exists, which is assigned as the $C_2H_3^+$ fragment ion. The kinetic energy release in dissociation causes the peak profile of $C_2H_3^+$ to apparently expand to 508 ns at full-width. No $C_2H_3Cl^+$ parent ions are observed, indicating that the $C_2H_3Cl^+(B^2A'')$ ion is fully dissociative. As indicated in the above reactions 1−5, only the Cl-loss and HCl formation channels are feasible at 13.14 eV. Both $C_2H_3^+$ and $C_2H_2^+$ fragment ions from these two channels were detected in previous TPEPICO[18] and MIKES experiments.[19] However, in the MATI-PDY experiment, only the $C_2H_3^+$ fragment was detected from the dissociation of the state-specific $C_2H_3Cl^+(B^2A'')$ ion.[12] Our results are consistent with the latter. Since the branching ratio of the HCl formation pathway (1) is much lower than that of the Cl-loss channel (2) in the previous experiments,[18,19] $C_2H_2^+$ ions are probably too weak to be observed and contribute an indistinct and weak shoulder in the broad TOF peak of $C_2H_3^+$ ions in Figure 4. In addition, very few $C_2H_2Cl^+$ fragment ions were observed in the energy range of 12.47−12.59 eV in the previous TPEPICO studies.[18] The photon energies in Figure 4 are out of the range, and thus it is reasonable not to observe $C_2H_2^+$ fragment ions.

Similar to the case at 13.14 eV, only a broad mass peak of $C_2H_3^+$ is detected in the TPEPICO TOF mass spectrum at 13.65 eV, as shown in Figure 4c. The peak profile of $C_2H_3^+$ is broadened to 620 ns at full-width, with a nearly triangular shape. Therefore, the Cl-loss pathway (2) also dominates, producing the $C_2H_3^+$ fragment ion at 13.65 eV. In addition, both the triangular profiles of $C_2H_3^+$ ion in Figure 4b,c suggest that the statistical dissociation is an important component in dissociation of $C_2H_3Cl^+$ ion in the B^2A'' and C^2A' states.

3.5. TPEPICO Three-Dimensional Time-Sliced Velocity Map Images of the $C_2H_3^+$ Fragment.

When the excitation energy is above the dissociation limit, fragmentation of $C_2H_3Cl^+$ can occur. As observed by Lee and Kim,[12] the $C_2H_3Cl^+(B^2A'')$ ion at a low vibrational excitation statistically dissociated to $C_2H_3^+$ and Cl fragments, while a non-statistical process occurred for the highly vibrationally excited B^2A'' state. However, the previous theoretical calculations provided inconsistent explanations for the dissociation mechanisms of $C_2H_3Cl^+$ in the B^2A'' and C^2A' states. As the inconsistency mainly focused on the role of the C^2A' state in dissociation of the near B^2A'' state, we pay special attention to dissociation of highly vibrationally excited $C_2H_3Cl^+(B^2A'')$ ions and selected a photon of 13.14 eV. As shown in the mass spectra of Figure 4b, the full-width of the $C_2H_3^+$ TOF profile expanded to 508 ns when an extraction electric field of 14 V·cm^{-1} was used. Thus, using a mass gate of 40 ns duration time for images centered at 10.67 μs can give a time-sliced effect. As the time-sliced portion of ion distribution is less than 8%, a three-dimensional (3D) time-sliced velocity map image can be directly recorded without inverse Abel transformation.[43] As the raw images are inevitably expanded along the flow direction of the molecular beam due to its velocity spread, the kinetic energy distribution of the fragment ions needs to be deconvoluted to counter the velocity spread and provide accurate data. The detailed data processing procedure can be found in the Supporting Information of ref 27.

Figure 5a shows the recorded TPEPICO 3D time-sliced velocity map image of $C_2H_3^+$ fragment ions at 13.14 eV, where the electric vector ε of a VUV photon is vertical in the image
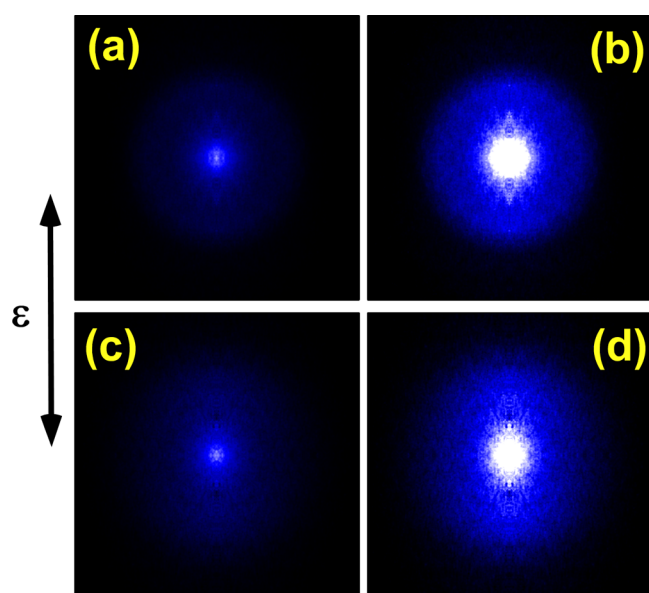
Figure 5. TPEPICO 3D time-sliced velocity map images of $C_2H_3^+$ fragment ions at (a, b) 13.14 and (c, d) 13.65 eV. The electric vector ε of a VUV photon is vertical in the image plane. (b, d) Images with a saturated color scale, to exhibit details of the outer image more clearly.

plane. No clear ring structure was observed, and the intensity of the center part was strong. A saturated color scale was applied to exhibit details of the outer image more clearly, and the resulting image is shown in Figure 5b. Unlike the center of the image, some parallel distribution along ε can be seen in the outer component. Similarly, the TPEPICO 3D time-sliced velocity map image of $C_2H_3^+$ was recorded at 13.65 eV, which is above the vertical ionization energy of the C^2A' state, and is presented, with the same use of different color scales as described above, in Figure 5c,d. Compared with those at 13.14 eV, a wider distribution and a more obvious parallel distribution was found for the outer image.

The speed distribution of $C_2H_3^+$ fragment was obtained by accumulating the intensity of the image over multiple angles. The total kinetic energy release distributions (KERD) in the dissociation of $C_2H_3Cl^+$ can be derived from the conservation of linear momentum. Figure 6a,b plots the total KERD curves

at 13.14 and 13.65 eV, respectively. At 13.14 eV, the total KERD curve shows an asymmetric profile with a shoulder at the lower energy, which is similar to the result of the MATI-PDY experiment at 13.061 eV.[12] Thus, the lower-energy shoulder is attributed to the contribution of statistical dissociation. The phase space theory (PST)[44] was used to fit the statistical component. The translational and rotational temperatures of the molecular beam were found to be ~20 K by analyzing the X- and Y-axis intensity distributions of the TPEPICO image of $C_2H_3Cl^+$ parent ions at 11.67 eV; the procedural details are provided in the Supporting Information. Using molecular parameters calculated at the B3LYP/6-311+G(d,p) level, for example, vibrational frequencies and rotational constants, the statistical KERD of Boltzmann profile is calculated and plotted in Figure 6a. The total KERD can be fitted very well with this Boltzmann profile and one Gaussian curve. As shown in Figure 6a, the shoulder is mainly contributed by statistical dissociation. The Gaussian profile distribution occupies a large proportion of the total KERD, with its center at 0.21 eV, indicating that the non-statistical dissociation pathway dominates at 13.14 eV. With a dissociation limit of 12.53 eV, the excess energy at 13.14 eV is 0.61 eV. However, the maximum released kinetic energy is only 0.46 eV in Figure 6a, and thus the $C_2H_3^+$ fragment ion is expected to be vibrationally excited in the dissociation process. Unfortunately, the tunneling of three protons caused uncertainty in the geometry of the ground-state $C_2H_3^+$ cation, which could take the Y-shape and bridge-type structures.[45−47] Thus, the vibrational population of $C_2H_3^+$ after dissociation is too complicated to be accurately determined, which makes the image structureless. Although the detailed vibrational population of the $C_2H_3^+$ fragment cannot be derived, the dissociative photoionization process of C_2H_3Cl at 13.14 eV could still be clarified. Additionally, the dissociation channels that produce a Cl atom in the $^2P_{1/2}$ and $^2P_{3/2}$ spin−orbit levels cannot be discerned in the present image.

Comparing with the KERD at 13.14 eV, the KERD at 13.65 eV extends more widely, with a long tail toward greater kinetic energies. Similarly, we calculated the released kinetic energy from statistical dissociation along the Cl-loss potential energy curve of the ground ionic state at 13.65 eV using PST, which is shown as a Boltzmann-type curve in Figure 6b. The higher excess energy means that the Boltzmann curve shows a wider
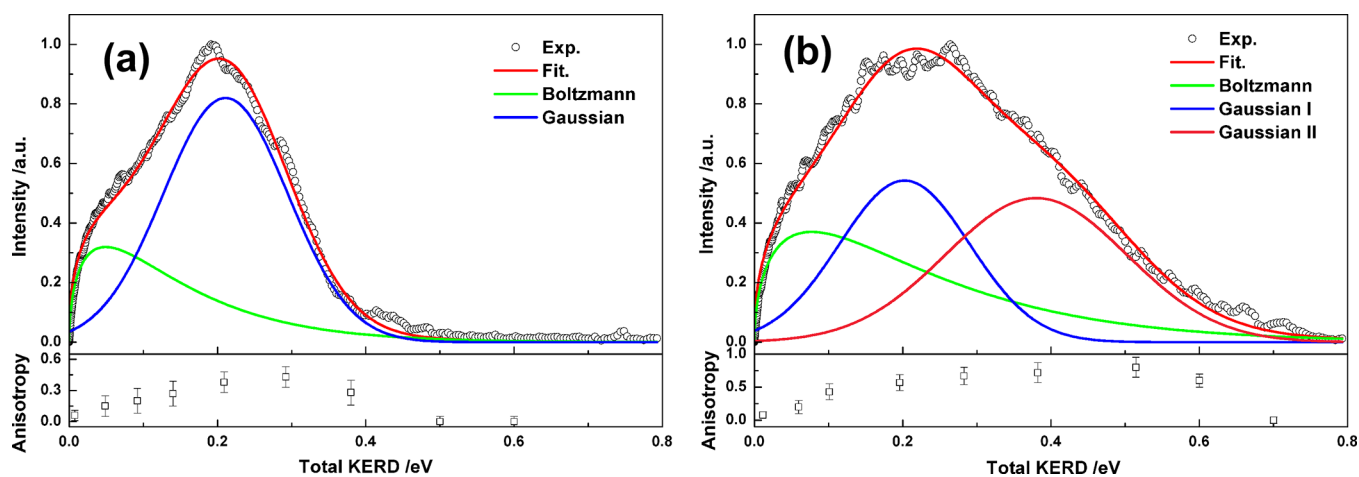

Figure 6. Total kinetic energy release distributions and anisotropy parameters of $C_2H_3^+$ fragment ions at (a) 13.14 and (b) 13.65 eV. The least-squares fittings of the total KERD curves are plotted with solid red lines.

Table 2. Branching Ratios and Anisotropy Parameters (β) of Statistical and Non-Statistical Dissociation Components for $C_2H_3^+$ Fragment Dissociated from State-Specific $C_2H_3Cl^+$ Ion

$h\nu$, eV	E_{avail}, eV[a]	component	branching ratio	$\langle E_T \rangle$, eV	f_T[b]	β
13.14 (B^{2}A″)	0.61	Boltzmann	36%	0.10	0.16	0.15 ± 0.10
		Gaussian	64%	0.21	0.34	0.38 ± 0.12
13.65 (C^{2}A′)	1.12	Boltzmann	38%	0.15	0.13	0.20 ± 0.10
		Gaussian I	33%	0.20	0.18	0.57 ± 0.12
		Gaussian II	29%	0.38	0.34	0.80 ± 0.15

[a]Available energy in dissociation of $C_2H_3Cl^+$ ion to $C_2H_3^+$ fragment. [b]Fraction of translation energy in total available energy, $f_T = \langle E_T \rangle / E_{avail}$.

distribution. To our surprise, no satisfactory fitting could be achieved with a combination of the Boltzmann curve and one Gaussian-type distribution, as done in Figure 6a. Therefore, an additional non-statistical dissociation path is expected at 13.65 eV, and combining the Boltzmann curve with two Gaussian-type distributions fit the experimental data very well. The overall fitting curve is presented in Figure 6b as a solid red line. The centers of the two Gaussian distributions locate at 0.20 and 0.38 eV, respectively.

From the images in Figure 5, the angular distribution of $C_2H_3^+$ fragment ions can be derived by integrating the images over an appropriate range of speed at each angle. Consequently, the anisotropy parameter β of $C_2H_3^+$ fragment ions produced from dissociation along different channels can be calculated by fitting the angular distribution $I(\theta)$ with the following formula 6
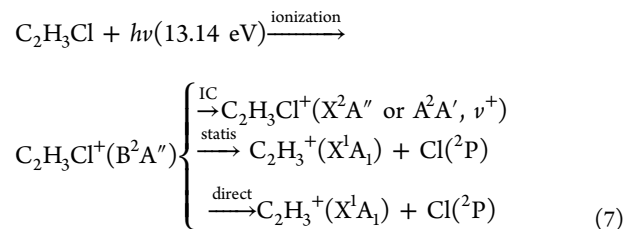
$$I(\theta) = \frac{1}{4}[1 + \beta \cdot P_2(\cos\theta)] \tag{6}$$

where θ is the angle between the recoil velocity of the fragment and the electric field vector ε of the VUV photon, and $P_2(\cos\theta)$ is the second-order Legendre polynomial. The fitted anisotropy parameters β of $C_2H_3^+$ cations at various released kinetic energy are also plotted in Figure 6. With increasing released kinetic energy, the β values gradually increased from zero to a positive value and then dramatically dropped at both 13.14 and 13.65 eV. For the lower KERD, β values are close to zero and consistent with its characteristic of statistical dissociation. For the Gaussian-type distributions at the higher KERD, β is 0.38 for the non-statistical components at 13.14 eV, which is slightly lower than the value in the MATI-PDY experiment.[12] At 13.65 eV, the β values increased to 0.57 and 0.80, respectively, for the two Gaussian distributions in the KERD of Figure 6b. The moderately positive values of β indicate that the overall dissociation process is faster than molecular rotation and agrees with its role in non-statistical dissociation. In addition, it is interesting that both β values are positive at 13.14 and 13.65 eV, although the B^{2}A″ and C^{2}A′ ionic states have different symmetries. In C_s symmetry, the parallel transition from the ground state of A″ to the excited state B^{2}A″ leads to a positive anisotropy parameter β, which agrees with our experimental results. However, a negative β value is expected for the perpendicular transition from the ground A″ state to the C^{2}A′ state, which is the opposite of our experimental conclusion. A brief discussion will be given in the following section, based on the dissociation mechanisms.
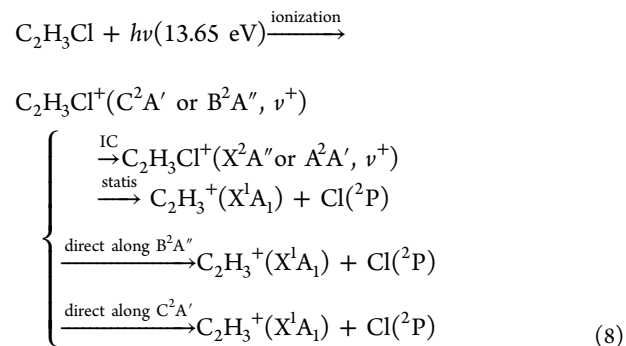
On the basis of the KERD fitting curves, branching ratios of the statistical and non-statistical dissociation pathways are calculated and summarized in Table 2. At 13.14 and 13.65 eV, the non-statistical dissociation remains dominant, with an almost constant branching ratio of 60%.

3.6. Dissociation Mechanisms of $C_2H_3Cl^+$ in the B^{2}A″ and C^{2}A′ States. With the aid of the calculated potential energy curves in Figure 2, the dissociation mechanisms of $C_2H_3Cl^+$ cation in the B^{2}A″ and C^{2}A′ states can be illuminated. Although it is very difficult to directly calculate the intensity of the B^{2}A″ and C^{2}A′ states in TPES from the ground state of the neutral molecule, their band profiles must be very different because of their different geometries. The C^{2}A′ state has a similar planar structure to the ground state of the neutral molecule, and thus the original band of C^{2}A′ is thought to show the stronger intensity in TPES. According to the calculated excitation energies in Table 1, the C^{2}A′ band should start from ~13.5 eV. Therefore, at 13.14 eV, the $C_2H_3Cl^+$ ion is prepared in its B^{2}A″ excited state. As its internal energy exceeds the adiabatic barrier to C−Cl bond cleavage, two competing pathways for Cl-loss mechanism are open: the first is a statistical dissociation via internal conversion to the X^{2}A″ or A^{2}A′ states, and the second is dissociation by overcoming the reverse barrier. The latter is anisotropic, and agrees very well with our experimental conclusion. Thus, these dissociation pathways are consistent with the two components of the KERD curve in Figure 6a. The overall dissociative photoionization mechanism at 13.14 eV can be summarized as the following:

$$C_2H_3Cl + h\nu(13.14\ eV) \xrightarrow{ionization}$$

$$C_2H_3Cl^+(B^2A'')\begin{cases} \xrightarrow{IC} C_2H_3Cl^+(X^2A''\ or\ A^2A',\ v^+) \\ \xrightarrow{statis} C_2H_3^+(X^1A_1) + Cl(^2P) \\ \xrightarrow{direct} C_2H_3^+(X^1A_1) + Cl(^2P) \end{cases} \tag{7}$$

Dissociative photoionization of C_2H_3Cl becomes more complicated at 13.65 eV. As indicated in Figure 2, highly vibrationally excited B^{2}A″ and C^{2}A′ states of $C_2H_3Cl^+$ can be produced at 13.65 eV. In the Franck−Condon region, the distance between the Cl and C atoms of $C_2H_3Cl^+$ ion quickly increases due to the repulsive force from the steep potential curves of the B^{2}A″ and C^{2}A′ states. As the internal energy is beyond the adiabatic barriers of both the B^{2}A″ and C^{2}A′ states, direct C−Cl bond rupture naturally proceeds. Thus, the overall dissociative photoionization mechanism is shown in eq 8.

$$C_2H_3Cl + h\nu(13.65\ eV) \xrightarrow{ionization}$$

$$C_2H_3Cl^+(C^2A'\ or\ B^2A'',\ v^+)$$

$$\begin{cases} \xrightarrow{IC} C_2H_3Cl^+(X^2A''or\ A^2A',\ v^+) \\ \xrightarrow{statis} C_2H_3^+(X^1A_1) + Cl(^2P) \\ \xrightarrow{direct\ along\ B^2A''} C_2H_3^+(X^1A_1) + Cl(^2P) \\ \xrightarrow{direct\ along\ C^2A'} C_2H_3^+(X^1A_1) + Cl(^2P) \end{cases} \tag{8}$$

On the basis of this mechanism, three components in the KERD curve of Figure 6b can be assigned. The statistical dissociation of the Boltzmann distribution corresponds to the first mechanism of eq 8. As the second fast channel originates from adiabatic dissociation of the B^2A'' state, the fraction of translation energy in the total available energy, $f_T = \langle E_T \rangle / E_{avail}$, should be close to the value at 13.14 eV. As indicated in Table 2, the Gaussian II component has the same f_T value as it has at 13.14 eV (~0.34). Thus, the Gaussian-type II distribution (in Table 2) is believed to be generated by the dissociation of the highly vibrationally excited B^2A'' state along its adiabatic potential energy curve. In general, for direct dissociation over the reverse barrier, a higher internal energy leads to a faster dissociation rate. Thus, a larger β value (0.80 for Gaussian-type II component) is observed at 13.65 eV than that at 13.14 eV (β = 0.38), which is consistent with our prediction.

The third C−Cl bond rupture mechanism is via adiabatic dissociation along the potential energy curve of the C^2A' state. As indicated in Figure 2, the excess energy of a $C_2H_3Cl^+$ ion in the Franck−Condon region is higher than the adiabatic barrier at 13.65 eV. Thus, adiabatic dissociation via intramolecular vibrational redistribution (IVR) is feasible and contributes to the Gaussian-type I distribution of the KERD in Figure 6b. The dissociation rate should be slower than the second mechanism because of the higher barrier of the C^2A' state. Thus, the partial excess energy of the C^2A' state is released before dissociation because of IVR in the well during the relatively long dissociation period. Therefore, the average translation energy of the Gaussian-type I component is lower than the Gaussian-type II part, which is consistent with our experimental conclusions. In addition, it is interesting that a negative β value is expected for a perpendicular transition to the C^2A' state in the dissociative process mentioned above. However, the contributions of the statistical dissociation (β = 0) and the parallel transition to the B^2A'' state (β > 0) cannot be ignored at 13.65 eV, as the spectral overlap in TPES. Thus, the average β value obtained for the Gaussian-type I component in the KERD is reduced to only 0.57 at 13.65 eV and is smaller than that of the Gaussian-type II (β = 0.80).

Although it is impossible for us to assess the population fractions of C^2A' and highly vibrationally excited B^2A'' states at 13.65 eV because of the overlapping spectral structure, it should be emphasized that a new direct dissociation pathway has been found, besides the statistical and non-statistical dissociations at 13.14 eV. Therefore, the C^2A' state plays an important role in the dissociation dynamics of the nearby highly vibrationally excited B^2A'' state.

4. CONCLUSIONS

Using VUV synchrotron radiation as a light source, dissociative photoionization of C_2H_3Cl in the excitation energy range of 11.0−14.5 eV was investigated by TPEPICO velocity map imaging of the A^2A', B^2A'', and C^2A' electronic states of $C_2H_3Cl^+$. Only the $C_2H_3{}^{35}Cl^+$ and $C_2H_3{}^{37}Cl^+$ molecular ions, with a natural abundance ratio, existed in the TPEPICO mass spectrum at 11.67 eV, indicating that the A^2A' state is bound as reported previously.[13] Although the HCl formation channel is an energetically accessible C−Cl cleavage path, only the $C_2H_3{}^+$ fragment ion was detected in TPEPICO mass spectra at 13.14 and 13.65 eV. No parent ions existed at these photon energies, implying that both the B^2A'' and C^2A' states are fully dissociative.

From the recorded TPEPICO 3D time-sliced images of $C_2H_3{}^+$ fragment ions, the KERD and anisotropy parameters in dissociation of the $C_2H_3Cl^+$ ion were obtained at 13.14 and 13.56 eV, respectively. At 13.14 eV, $C_2H_3Cl^+$ was prepared purely in the B^2A'' state, and its total KERD exhibited a bimodal distribution. A Boltzmann distribution calculated with PST and one Gaussian-type curve were combined fitting the KERD curve very closely. Competition between statistical and non-statistical processes was suggested to occur during its dissociation. The total KERD curve at 13.65 eV needed to be fitted with one Boltzmann distribution and two Gaussian-type curves. Therefore, a new dissociation pathway exists for the $C_2H_3Cl^+$ cation in the C^2A' state or highly vibrationally excited B^2A'' state.

The optimized geometries of the low-lying electronic states of $C_2H_3Cl^+$ were reinvestigated using the TD-DFT B3LYP/6-311+G(d,p) level of theory. Using the optimized geometries, the vertical and adiabatic ionization energies of the ionic states were calculated at the EOM-CCSD/cc-PVTZ level. The Cl-loss potential energy curves of the X^2A'', A^2A', B^2A'', and C^2A' states were calculated at TD-DFT B3LYP/6-311+G(d,p) level as well. The B^2A'' state has a twisted geometry, and the optimized C−Cl bond length is far from the Franck−Condon region. A small barrier exists for the B^2A'' state with a low height of 0.06 eV along the C−Cl distance. The adiabatic dissociation products of $C_2H_3Cl^+(B^2A'')$ ions were $C_2H_3{}^+(X^1A_1)$ and $Cl(^2P)$ as well as those of X^2A'' and A^2A' states. The C^2A' state has a similar planar geometry to the ground state of the neutral molecule and adiabatically correlates with the $C_2H_3{}^+(X^1A_1) + Cl(^2P)$ production via a small barrier of 0.10 eV.

On the basis of the Cl-loss potential energy curves, dissociative photoionization mechanisms for C_2H_3Cl at 13.14 and 13.65 eV via the B^2A'' and C^2A' ionic states were obtained. Two competing pathways for the Cl-loss dissociation process were found at 13.14 eV: a statistical dissociation via internal conversion to the ground state (or A^2A') and an adiabatic dissociation by overcoming the reverse barrier. At 13.65 eV, the dissociation mechanism becomes more complicated, since both the highly vibrationally excited B^2A'' state and the C^2A' state are probably produced. The statistical dissociation still existed at 13.14 eV. Two types of fast dissociation mechanisms were suggested for the $C_2H_3Cl^+$ cation: first, adiabatic dissociation along the potential energy curve of B^2A'' as was the case at 13.14 eV, and second, dissociation along the adiabatic potential energy curve of the C^2A' state. Because of the higher reverse barrier, the latter had a slower dissociation rate. Thus, the partial excess energy of the C^2A' state can be released by IVR before its dissociation, and the average released translation energy of this channel was lower. In addition, curve-crossing may result in a strong coupling between the B^2A'' and C^2A' states, and thus the present assignment of two Gaussian-type distributions is somewhat rough. More experimental data are necessary, especially in the excitation energy range below the barrier of C^2A' state. However, we can say with certainty that the C^2A' state plays an important role in the dissociation dynamics of the nearby B^2A'' state.

■ ASSOCIATED CONTENT

ⓢ Supporting Information

The Supporting Information is available free of charge on the ACS Publications website at DOI: 10.1021/acs.jpca.7b03636.

Potential energy curves, discussion of translational temperature of the molecular beam (PDF)

■ AUTHOR INFORMATION

Corresponding Author
*E-mail: xzhou@ustc.edu.cn.

ORCID ⊙
Xiaoguo Zhou: 0000-0002-0264-0146

Author Contributions
‖These authors contributed equally to this work.

Notes
The authors declare no competing financial interest.

■ ACKNOWLEDGMENTS

■ REFERENCES

(1) Sood, S. P.; Watanabe, K. Absorption and Ionization Coefficients of Vinyl Chloride. *J. Chem. Phys.* **1966**, *45*, 2913−2915.

(2) Locht, R.; Leyh, B.; Hottmann, K.; Baumgärtel, H. The Photoabsorption Spectrum of Vinylchloride (C_2H_3Cl) in the 8−12 eV Range. *Chem. Phys.* **1997**, *220*, 207−216.

(3) Limao-Vieira, P.; Vasekova, E.; Sekhar, B. N. R.; Mason, N. J.; Hoffmann, S. V. VUV Photo-absorption Spectroscopy of Vinyl Chloride Studied by High Resolution Synchrotron Radiation. *Chem. Phys.* **2006**, *330*, 265−274.

(4) Williams, B. A.; Cool, T. A. Resonance Ionization Spectroscopy of the Chloroethylenes. *J. Phys. Chem.* **1993**, *97*, 1270−1282.

(5) Chang, J. L.; Shieh, J. C.; Wu, J. C.; Li, R. H.; Chen, Y. T. High-lying Rydberg States and Ionization Energy of Vinyl Chloride Studied by Two-photon Resonant Ionization Spectroscopy. *Chem. Phys. Lett.* **2000**, *325*, 369−374.

(6) Kishimoto, N.; Ohshimo, K.; Ohno, K. Penning Ionization of Vinyl Chloride and Vinyl Iodide by Collision with He*(2^3S) Metastable Atoms. *J. Electron Spectrosc. Relat. Phenom.* **1999**, *104*, 145−154.

(7) Von Niessen, W.; Åsbrink, L.; Bieri, G. 30.4 nm He (II) Photoelectron Spectra of Organic Molecules Part VI. Halogeno-compounds (C, H, X; X= Cl, Br, I). *J. Electron Spectrosc. Relat. Phenom.* **1982**, *26*, 173−201.

(8) Sze, K. H.; Brion, C. E.; Katrib, A.; El-Issa, B. Excitation and Ionization of the Monohaloethylenes (C_2H_3X, X= F, Cl, Br, I). II. Photoionization by He (I) and He (II) Photoelectron Spectroscopy and Valence-shell Excitation by Electron Energy Loss Spectroscopy. *Chem. Phys.* **1989**, *137*, 369−390.

(9) Locht, R.; Leyh, B.; Hottmann, K.; Baumgärtel, H. The He (I), Threshold Photoelectron and Constant Ion State Spectroscopy of Vinylchloride (C_2H_3Cl). *Chem. Phys.* **1997**, *220*, 217−232.

(10) Zhang, P.; Li, J.; Mo, Y. Vibrational Structure of Vinyl Chloride Cation Studied by Using One-photon Zero-kinetic Energy Photo-electron Spectroscopy. *J. Phys. Chem. A* **2007**, *111*, 8531−8535.

(11) Lee, M.; Kim, M. S. Mass-analyzed Threshold Ionization Study of Vinyl Chloride Cation in the First Excited Electronic State Using Vacuum Ultraviolet Radiation in the 107−102.8 nm Range. *J. Phys. Chem. A* **2006**, *110*, 9377−9382.

(12) Lee, M.; Kim, M. S. Vibrational Spectroscopy and State-Specific Dissociation Dynamics for Vinyl Chloride Cation in the B̃ State. *J. Phys. Chem. A* **2007**, *111*, 8409−8415.

(13) Youn, Y. Y.; Choe, J. C.; Kim, M. S. Discovery of Long-lived Excited Electronic States of Vinylchloride, Vinylbromide, Vinyliodide, and Acrylonitrile Cations. *J. Am. Soc. Mass Spectrom.* **2003**, *14*, 110−116.

(14) Reinke, D.; Kraessig, R.; Baumgärtel, H. Photoreactions of Small Organic Molecules. *Z. Naturforsch., A: Phys. Sci.* **1973**, *28*, 1021−1031.

(15) Zhang, Y. W.; Sheng, L. S.; Qi, F.; Gao, H.; Yu, S. Q. Photoionization Studies of Some Small Molecules. *J. Electron Spectrosc. Relat. Phenom.* **1996**, *79*, 483−485.

(16) Sheng, L. S.; Qi, F.; Gao, H.; Zhang, Y.; Yu, S. Q. Vacuum-ultraviolet Photoion Spectrum of Vinyl Chloride Near Ionization Threshlod. *Acta Phys. Chim. Sin.* **1997**, *7*, 014.

(17) Sheng, L. S.; Qi, F.; Tao, L.; Zhang, Y.; Yu, S. Q.; Wong, C. K.; Li, W. K. Experimental and Theoretical Studies of the Photoionization and Dissociative Photoionizations of Vinyl Chloride. *Int. J. Mass Spectrom. Ion Processes* **1995**, *148*, 179−189.

(18) Shuman, N. S.; Ochieng, M. A.; Sztáray, B.; Baer, T. TPEPICO Spectroscopy of Vinyl Chloride and Vinyl Iodide: Neutral and Ionic Heats of Formation and Bond Energies. *J. Phys. Chem. A* **2008**, *112*, 5647−5652.

(19) Yoon, S. H.; Choe, J. C.; Kim, M. S. Anisotropic Photo-dissociation of Vinyl Chloride Molecular Cation in the Ground and First Excited Electronic States. *Int. J. Mass Spectrom.* **2003**, *227*, 21−32.

(20) Chang, H. B.; Chen, B. Z.; Huang, M. B. Low-lying Electronic States and Cl-loss Photodissociation of the $C_2H_3Cl^+$ Ion Studied Using Multiconfiguration Second-order Perturbation Theory. *J. Phys. Chem. A* **2008**, *112*, 1688−1693.

(21) Yamaguchi, M. Multireference Configuration Interaction Study of the Vibronic Transitions and Photodissociation of Vinyl Bromide and Vinyl Chloride Radical Cations in the Second Excited State. *J. Phys. Chem. A* **2010**, *114* (30), 7937−7944.

(22) Tang, X. F.; Zhou, X. G.; Niu, M. L.; Liu, S. L.; Sun, J. D.; Shan, X. B.; Liu, F. Y.; Sheng, L. S. A Threshold Photoelectron-photoion Coincidence Spectrometer with Double Velocity Imaging Using Synchrotron Radiation. *Rev. Sci. Instrum.* **2009**, *80*, 113101.

(23) Garcia, G. A.; Soldi-Lose, H.; Nahon, L. A Versatile Electron-ion Coincidence Spectrometer for Photoelectron Momentum Imaging and Threshold Spectroscopy on Mass Selected Ions Using Synchrotron Radiation. *Rev. Sci. Instrum.* **2009**, *80*, 023102.

(24) Bodi, A.; Johnson, M.; Gerber, T.; Gengeliczki, Z.; Sztáray, B.; Baer, T. Imaging Photoelectron Photoion Coincidence Spectroscopy with Velocity Focusing Electron Optics. *Rev. Sci. Instrum.* **2009**, *80*, 034101.

(25) Bodi, A.; Hemberger, P.; Gerber, T.; Sztáray, B. A New Double Imaging Velocity Focusing Coincidence Experiment: i2PEPICO. *Rev. Sci. Instrum.* **2012**, *83*, 083105.

(26) Garcia, G. A.; Cunha de Miranda, B. K.; Tia, M.; Daly, S.; Nahon, L. DELICIOUS III: A Multipurpose Double Imaging Particle Coincidence Spectrometer for Gas Phase Vacuum Ultraviolet Photodynamics Studies. *Rev. Sci. Instrum.* **2013**, *84*, 053112.

(27) Tang, X. F.; Niu, M. L.; Zhou, X. G.; Liu, S. L.; Liu, F. Y.; Shan, X. B.; Sheng, L. S. NO+ Formation Pathways in Dissociation of N_2O^+ Ions at the $C^2\Sigma+$ State Revealed from Threshold Photoelectron− Photoion Coincidence Velocity Imaging. *J. Chem. Phys.* **2011**, *134*, 054312.

(28) Tang, X. F.; Zhou, X. G.; Niu, M. L.; Liu, S. L.; Sheng, L. S. Dissociation of Vibrational State-Selected O_2^+ Ions in the $B^2\Sigma_g^-$ State Using Threshold Photoelectron−Photoion Coincidence Velocity Imaging. *J. Phys. Chem. A* **2011**, *115*, 6339−6346.

(29) Tang, X. F.; Zhou, X. G.; Wu, M. M.; Cai, Y.; Liu, S. L.; Sheng, L. S. Direct Experimental Evidence for Dissociative Photoionization of Oxygen Molecule via $^2\Sigma_u^-$ Ionic "Optical Dark" State. *J. Phys. Chem. A* **2012**, *116*, 9459−9465.

(30) Tang, X. F.; Zhou, X. G.; Wu, M. M.; Liu, S. L.; Liu, F. Y.; Shan, X. B.; Sheng, L. S. Dissociative Photoionization of Methyl Chloride Studied with Threshold Photoelectron-Photoion Coincidence Velocity Imaging. *J. Chem. Phys.* **2012**, *136*, 034304.

(31) Tang, X. F.; Zhou, X. G.; Wu, M. M.; Gao, Z.; Liu, S. L.; Liu, F. Y.; Shan, X. B.; Sheng, L. S. Dissociation Limit and Dissociation

Dynamic of CF_4^+: Application of Threshold Photoelectron-Photoion Coincidence Velocity Imaging. *J. Chem. Phys.* **2013**, *138*, 094306.

(32) Tang, X. F.; Zhou, X. G.; Sun, Z. F.; Liu, S. L.; Liu, F. Y.; Sheng, L. S.; Yan, B. Dissociation of Internal Energy-selected Methyl Bromide Ion Revealed from Threshold Photoelectron-Photoion Coincidence Velocity Imaging. *J. Chem. Phys.* **2014**, *140*, 044312.

(33) Tang, X. F.; Zhou, X. G.; Qiu, B. L.; Liu, S. L.; Liu, F. Y.; Shan, X. B.; Sheng, L. S. New Insight Into Dissociative Photoionization of N_2O at~ 20eV Using Threshold Photoelectron−Photoion Coincidence Velocity Imaging. *J. Electron Spectrosc. Relat. Phenom.* **2014**, *196*, 43−48.

(34) Sztáray, B.; Baer, T. Suppression of Hot Electrons in Threshold Photoelectron Photoion Coincidence Spectroscopy Using Velocity Focusing Optics. *Rev. Sci. Instrum.* **2003**, *74*, 3763−3768.

(35) Frisch, M. J.; Trucks, G. W.; Schlegel, H. B.; Scuseria, G. E.; Robb, M. A.; Cheeseman, J. R.; Scalmani, G.; Barone, V.; Mennucci, B.; Petersson, G. A., et al. *Gaussian 09W,* Revision D.1; Gaussian, Inc.: Wallingford, CT, 2009.

(36) Koch, H.; Jorgensen, P. Coupled Cluster Response Functions. *J. Chem. Phys.* **1990**, *93*, 3333−3344.

(37) Stanton, J. F.; Bartlett, R. J. The Equation of Motion Coupled-Cluster Method. A Systematic Biorthogonal Approach to Molecular Excitation Energies, Transition Probabilities, and Excited State Properties. *J. Chem. Phys.* **1993**, *98*, 7029−7039.

(38) Koch, H.; Kobayashi, R.; Sanchez de Merás, A.; Jorgensen, P. Calculation of Size-Intensive Transition Moments from the Coupled Cluster Singles and Doubles Linear Response Function. *J. Chem. Phys.* **1994**, *100*, 4393−4400.

(39) Kállay, M.; Gauss, J. Calculation of Excited-State Properties Using General Coupled-Cluster and Configuration-Interaction Models. *J. Chem. Phys.* **2004**, *121*, 9257−9269.

(40) Harvey, J.; Bodi, A.; Tuckett, R. P.; Sztáray, B. Dissociation Dynamics of Fluorinated Ethene Cations: from Time Bombs on A Molecular Level to Double-Regime Dissociators. *Phys. Chem. Chem. Phys.* **2012**, *14*, 3935−3948.

(41) Harvey, J.; Hemberger, P.; Bodi, A.; Tuckett, R. P. Vibrational and Electronic Excitations in Fluorinated Ethene Cations from the Ground Up. *J. Chem. Phys.* **2013**, *138*, 124301.

(42) Herzberg, G. Molecular Spectra and Molecular Structure. In *Electronic Spectra and Electronic Structure of Polyatomic Molecules;* Van Nostrand, Reinhold: New York, 1966; Vol. 3.

(43) Lin, J. J.; Zhou, J.; Shiu, W.; Liu, K. Application of Time-Sliced Ion Velocity Imaging to Crossed Molecular Beam Experiments. *Rev. Sci. Instrum.* **2003**, *74*, 2495−2500.

(44) Baer, T.; Hase, W. L. *Unimolecular Reaction Dynamics: Theory and Experiments;* Oxford University Press on Demand, 1996.

(45) Sharma, A. R.; Wu, J.; Braams, B. J.; Carter, S.; Schneider, R.; Shepler, B.; Bowman, J. M. Potential Energy Surface and Multimode Vibrational Analysis of $C_2H_3^+$. *J. Chem. Phys.* **2006**, *125*, 224306.

(46) Lindh, R.; Roos, B. O.; Kraemer, W. P. A CAS SCF CI Study of the Hydrogen Migration Potential in Protonated Acetylene, $C_2H_3^+$. *Chem. Phys. Lett.* **1987**, *139*, 407−416.

(47) Vager, Z.; Zajfman, D.; Graber, T.; Kanter, E. P. Experimental Evidence for Anomalous Nuclear Delocalization in $C_2H_3^+$. *Phys. Rev. Lett.* **1993**, *71*, 4319.